Svalbard snow and sea-ice cover: comparing satellite data, on-site measurements, and modelling results (SvalSCESIA)

Mari Anne Killie[1], Signe Aaboe[1], Ketil Isaksen[1], Ward Van Pelt[2], Åshild Ø. Pedersen[3], and Bartłomiej Luks[4]

[1] The Norwegian Meteorological Institute, Postboks 43 Blindern, 0371 Oslo, Norway
[2] Department of Earth Sciences, Uppsala University, SE-75236 Uppsala, Sweden
[3] The Norwegian Polar Institute, FRAM Centre, NO-9296 Tromsø, Norway
[4] Institute of Geophysics, Polish Academy of Sciences, Księcia Janusza 64, 01-452 Warsaw, Poland

Corresponding author: Mari Anne Killie, **mariak@met.no**
ORCID number 0000-0001-5594-2124

Keywords: In-situ, modelling, remote sensing, sea-ice area, snow cover extent

DOI: https://doi.org/10.5281/zenodo.4293804

1. Introduction

The presence of snow cover has a large impact on Arctic ecosystems, human activities, atmospheric processes and the Earth's surface energy balance. However, the snow cover is challenging to map for larger regions due to its large spatial and temporal variability and its changing properties influenced by temperature, precipitation, wind, vegetation and local topography. Also, the sparse number of weather stations with snow cover measurements contributes to a poor observational database. Svalbard is located on the border between the ice-covered Arctic Ocean and the warmer North Atlantic sector; therefore the sea becomes a controlling factor of the climate. By using satellite remote sensing monitoring, it is possible to get a better overview of the snow conditions on land.

In this study, we use existing long-term climate data records of the snow cover on Svalbard and the sea-ice area in the adjacent sea, based on satellite data, to investigate how they are related to each other. The long-term climate data record of the snow cover on Svalbard (Killie 2019) is combined with the snow model output for snow water equivalent and in-situ measurements of snow cover and snow-off dates. Temporal as well as spatial trends are investigated. From existing global satellite climate data records of sea-ice concentration, the sea-ice trends in a selected Svalbard region are investigated in relation to the snow cover trends.

2. Overview of existing data

The datasets contributing to this study include long-term satellite data records (section 2.1.1 and 2.1.4), long-term in-situ ground measurements (section 2.1.2), as well as output extracted from a long-term model dataset of climatic mass balance, snow conditions and runoff in Svalbard (section 2.1.3). We also include a shorter data record from in-situ measurements of ground surface temperature [COAT (Pedersen et al. 2020), section 2.1.2]. A common grid and overlapping time span are selected where possible. The satellite-based snow cover data record covers 1982–2015, and thus the sea-ice concentration data, in-situ ground data and snow modelling data are restricted to cover the same time period. Over land, the snow model data are re-projected to the same 4 km resolution grid as the satellite snow cover data record. The coastal zone is masked, and for quantitative analysis, glaciated land pixels are masked as well. Figure 1 shows land pixels (snow-covered or snow-free) and glaciated pixels. The inset map shows the regions used for comparison with in-situ data.

In section 2.1, the datasets are presented in separate sub-sections, and in the following section 2.2, potential correlations are investigated.

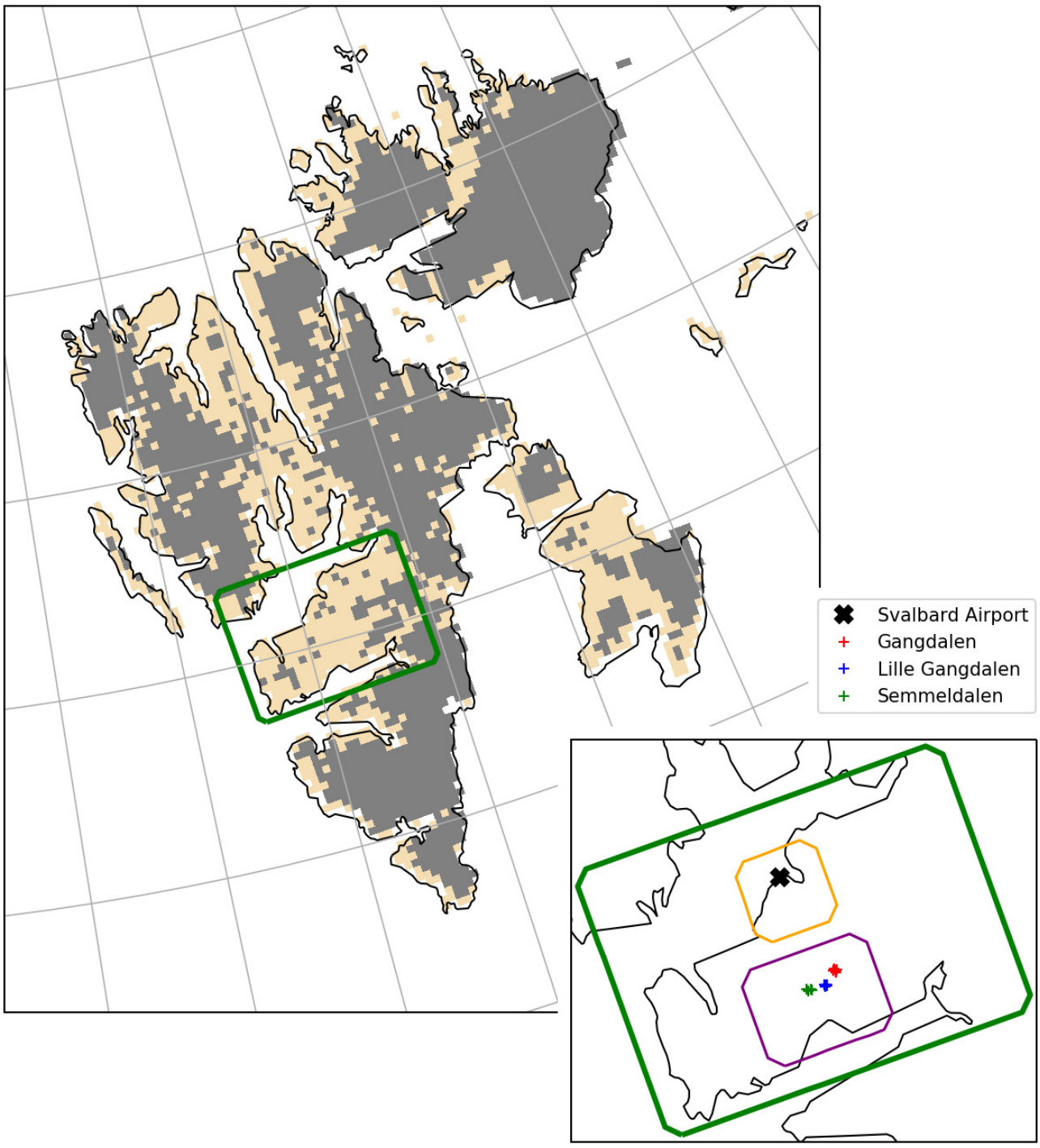

Figure 1: Map of Svalbard showing the study area in Central Spitsbergen. Glaciated pixels are shown in grey. The inserted map shows the regions that are used for comparison between the satellite snow product against in-situ snow cover data (orange square) observed at the manned weather station at Svalbard Airport (marked with a black marker), and against in-situ spatial data on snow-off dates (purple square) in three valleys on Nordenskiöld Land – Gangdalen, Lille Gangdalen and Semmeldalen – marked with red, blue, and green markers, respectively.

2.1 Dataset description

2.1.1 Satellite data for terrestrial snow

The Advanced Very High Resolution Radiometer (AVHRR) instrument is a versatile imaging instrument used for monitoring cloud cover, land and water surfaces. Sea surface temperature, snow cover, ice cover and vegetation characteristics are parameters that can be derived from AVHRR data. The instrument has flown onboard polar-orbiting satellites since the late 1970s. The resolution is approximately 1 km, but only data at a reduced resolution of approximately 4 km is permanently archived and available with Global Area Coverage (GAC). A Fundamental Climate Data Record (FCDR) for radiances and brightness temperatures from the AVHRR GAC data has been made available by the EUMETSAT Climate Monitoring Satellite Application Facility. The current FCDR covers 1982–2015 and is the basis for the satellite-based product for terrestrial snow cover discussed in this chapter. An updated FCDR, with an extended data period including 2020, is planned for release within 2021 and will allow for a larger overlap in time with more modern snow or snow-proxy in-situ observations, such as the in-situ data described in section 2.1.2.

MET Norway's probabilistic snow cover algorithm, normally used in conjunction with AVHRR data for the mainland of Norway (Killie et al. 2011), has been adjusted to be used for the Svalbard archipelago. The algorithm uses a set of signatures (instrument channel combinations) and statistical coefficients derived from training datasets of typical surface classes. Satellite swath products from 24 hours are aggregated into daily products at 4 km grid spacing, and a threshold at 50% probability for snow is set, giving a daily, binary snow/no snow product. This snow cover product has been validated against ground observations of snow depth from weather stations at Ny Ålesund, Svalbard Airport, Hornsund, Barentsburg, Bjørnøya and Sveagruva, and from samplings of snow depths across Nordenskiöld Land. The total hit rate for snow was in the 92–98% range for the different observation sites, and the total hit rate for snow-free land was in the 52–64% range. Representation error is a challenge when validating a 4 km satellite product against point observations. The location of the weather station does not necessarily represent the surrounding terrain well. This can be particularly challenging for Svalbard, which is characterized by a narrow coastal zone and steep terrain. In some cases, the ground observation is located near glaciers, and the corresponding satellite grid cell is dominated by the radiative properties of the glacier.

In addition to the relatively coarse resolution, AVHRR data are also limited by clouds. Due to frequent cloud cover in the Arctic regions, a 24-hour aggregation period is normally insufficient to give a cloud-free product for Svalbard. Therefore, the dataset contains a gap-filled product as well, where the nearest-in-time cloud-free information searching up to 9 days forward or backward in time is filled in when needed. In the following analysis, the gap-filled product is used.

The algorithm uses reflected sunlight from the surface, and only the pixels for which the solar elevation is 10 degrees or more above the horizon are processed. The Svalbard dataset is therefore constrained to March through September for each year of 1982–2015. This means that the melting season is well covered, but the onset of the snow season later than September is not covered. From this binary product, the following parameters can be derived: The number of snow-free days (SFD) is calculated for each pixel as the number of days with no snow over a time period of interest; the snow-covered fraction (SCF) is the ratio of snow-covered pixels to the total number of land pixels per day; and the land-covered fraction (LCF) is similarly the ratio of snow-free pixels to the total land pixels. The snow cover extent (SCE) shows the accumulated area of snow-covered pixels in square kilometres and is useful for comparing monthly or interannual variations.

In Figure 2, the upper right panel shows the SCF for each day in 1982–2015. A 9-days moving average has been applied to reduce high frequency noise. As seen by the seasonal time series, the melting detected from this dataset typically starts between the second half of May and end of June. The years are coloured depending on their decade and thereby indicate a shift towards an earlier melting start and advanced spring season. The lower right panel shows the trend of the melt onset by plotting for each year the day-of-year when the SCF falls below 95%. The linear trend of the melting onset is found to have a negative rate of 2.6 days per decade (significant to the 0.05 level). This corresponds to well a week earlier melt-start over the 30+ years of satellite data studied here.

Figure 3 shows the spatial distribution of the trend over the 1982–2015 period in the total SFD during May to August, as well as a histogram of all land pixels as a function of height, where the colour represents the trend values. About 77% of the pixels showing a significant trend have an increase in the number of snow-free days (red colour), while 23% show a decrease (blue colour). The areas of largest positive trends are concentrated in regions that are dominated by lowland valleys and coastal plains. Most noticeable are the trends centred near the large valleys on Nordenskiöld Land: Adventdalen, Reindalen and Sassendalen. Here, a positive trend in the range of 1 to 2 days per year is found. The areas with a decrease in SFD (blue regions) are less dependent on elevation.

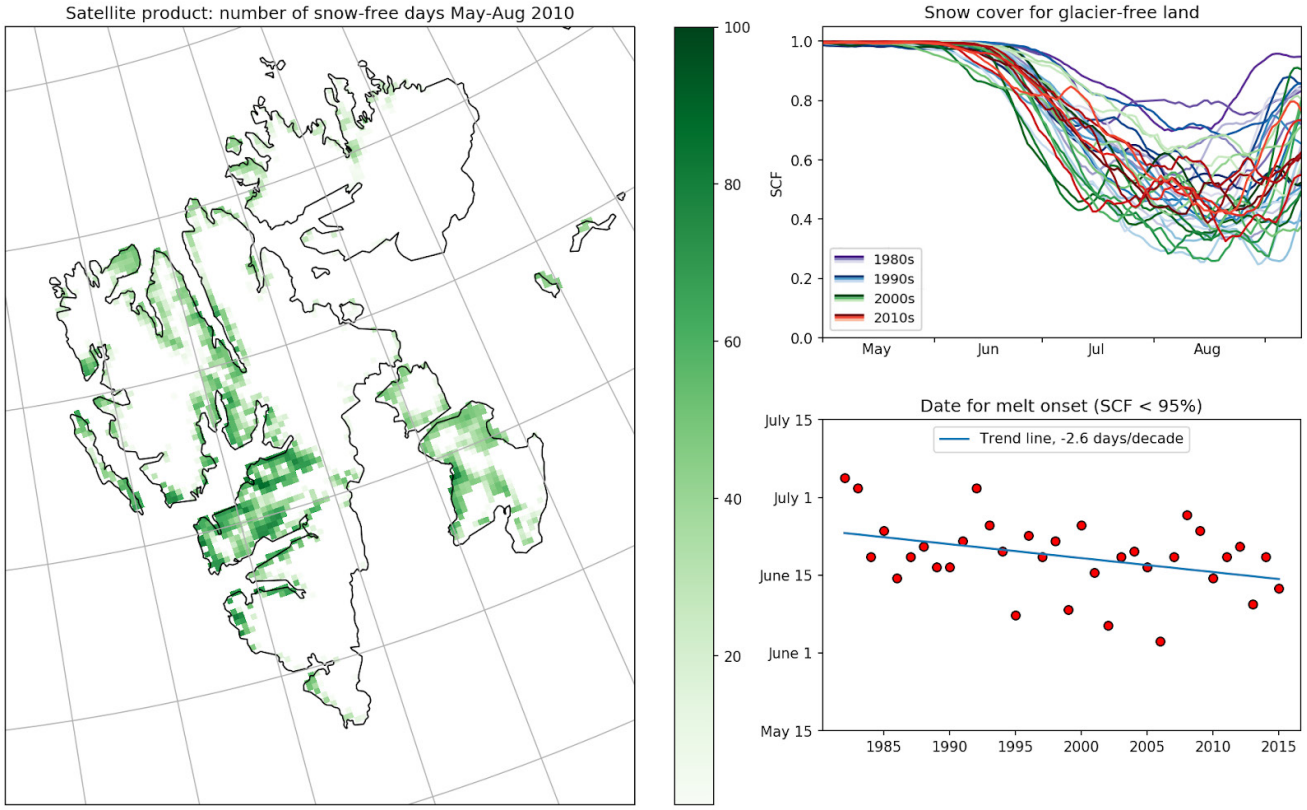

Figure 2: The left panel shows the number of snow-free days for the summer period May–August for 2010. The upper right panel shows the total ratio of snow-covered area (the SCF from which glacier areas are excluded) during May to mid-September. Each year of the 1982–2015 period is indicated by a separate line. A 9-days moving average has been applied. The lower right panel shows a scatter plot for the day-of-year for which the SCF shrinks below 95%, ref: upper right panel.

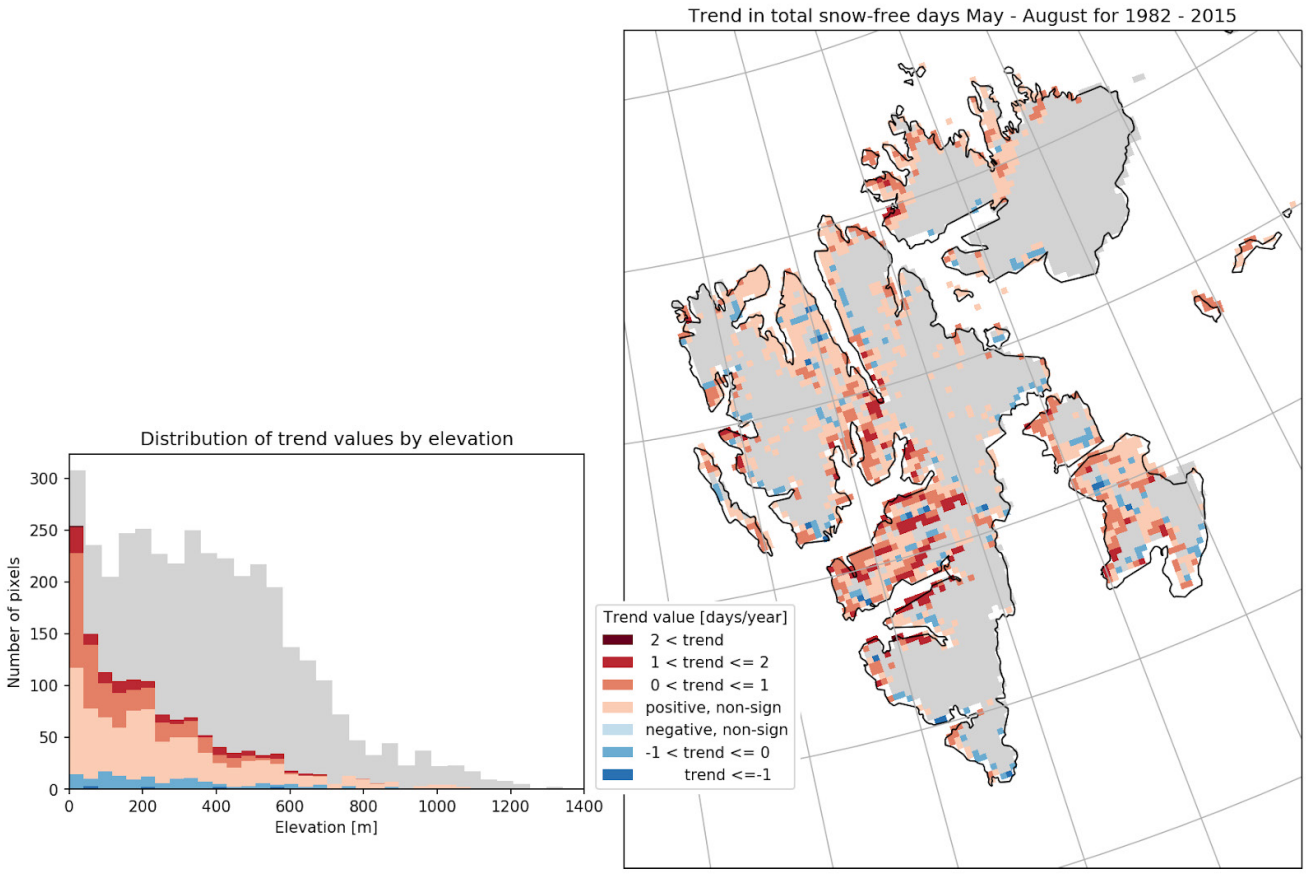

Figure 3: Right panel: Trend map in the total number of SFD from May to August over the 1982–2015 period. Grey areas are glaciated pixels (masked). Positive trends are shown in red, and negative trends are shown in blue. Non-significant trends are shown in light red/light blue. Left panel: The histogram shows the trend values as a function of elevation. The grey background shows how the glaciated pixels are distributed as a function of elevation.

2.1.2 In-situ data for snow

In this study, we use two different types of in-situ snow data: snow-off dates derived from temperature loggers from the COAT observation system and manually observed records for snow cover from a weather station. Both datasets are described briefly in this section and compared with the satellite snow product in section 2.2.1.

The long-term Climate-ecological Observatory for Arctic Tundra (COAT) observation system monitors several state variables, including the timing of snowmelt, locally in a network of temperature loggers on the ground surface (Ims et al. 2013). In 2009, a spatial design was implemented to cover the two most important Svalbard reindeer habitats (Loe et al. 2016). COAT builds on this and its own established network of loggers. “Ground surface temperature” is defined as the surface or near-surface temperature of the ground (bedrock or surficial deposit), as measured in the uppermost centimetres of the ground. Ground surface temperature data loggers are currently spatially widespread within the COAT regions on Nordenskiöld Land and along the west coast (Brøggerhalvøya and Forlandssundet). With the data from these loggers, it is possible to calculate the snow-off dates (c.f. Staub and Delaloye, 2017). Let’s take an example from three valleys on Nordenskiöld Land (see inset in Figure 1). Here, ground temperature loggers (iButton DS1921G; Maxim Integrated, San Jose, California, USA) have been placed in the soil surface in the ridge (dominated by *Salix polaris*) and sub-ridge vegetation (dominated by *Luzula confusa* and/or *Poa spp.*) at 48 locations, along elevational gradients throughout the study area. Ridge and sub-ridge vegetation types were selected because they constitute the main feeding habitat for reindeer in winter (Hansen et al. 2010). Wind-induced snow transport processes result in a strong heterogeneity of the winter snow cover (e.g. Luce

et al. 1998; Mott et al. 2012). The spatial variability of the snow depth distribution at the time of peak accumulation and the local energy balance result in a gradual development of a patchy snow cover during the ablation period (Mott et al. 2012). The COAT ridge and sub-ridge sites used here are exposed to wind, and snow depths are generally thinner (typically snow depth is 35 cm in March according to Loe et al. 2016) than those in other areas of the landscape where snow accumulates as deep drifts in sheltered spots and where it remains until early summer (snowbed communities). Thus, these sites must be regarded as sites representing early snow-off dates. Each logger recorded the soil surface temperature every fourth hour throughout the year with accuracy of 0.5 degrees C. Data description and protocols are further described in Loe et al. (2016).

In-situ observations of snow cover (SC) are manually performed by the Norwegian Meteorological Institute in a radius of 1 kilometre around the weather station at Svalbard Airport (see Figure 1). The observations are made in line with national and international guidelines for observations of snow cover. SC is an estimated assessment made by an observer and the results may be slightly dependent on the person. SC is reported using codes 0–4: 0 – No snow, 1 – Mostly bare ground, but some snow patches, 2 – Half the ground is snow covered, 3 – Mostly snow-covered ground, but some bare patches and 4 – Full snow cover.

2.1.3 Snow model data

Van Pelt et al. (2019) present a dataset of simulated glacier climatic mass balance, seasonal snow conditions and runoff for the entire land-area of Svalbard. Driven by a meteorological forcing from a regional climate model, the model solves the surface energy balance to estimate surface temperature and melt and simulates the multi-layer evolution of snow temperature, density and water content (Van Pelt et al. 2012; Van Pelt and Kohler 2015). For 1957–2018, Van Pelt et al. (2019) found, for Svalbard, a non-significant trend in snow disappearance date (0.0±0.9 days decade^{-1}) and a significant increase in snow onset date (1.4±0.9 days decade^{-1}). Here, the model output of snow water equivalent (SWE), including both seasonal snow and multi-year snow (firn), is used. The SWE data are projected from the original 1-km resolution model grid to the 4-km resolution satellite product grid by means of linear interpolation. From the SWE data, the number of SFD is calculated by assuming that snow-free conditions apply when SWE is below 0.01 m water equivalent. The snow model data is compared with the satellite-based snow cover product in section 2.2.2.

2.1.4 Satellite data for sea ice

For more than four decades, sea ice has been monitored in the polar regions by using satellite remote sensing. In this study, we use the global sea-ice concentration climate data record, version 2, from the EUMETSAT Ocean and Sea Ice Satellite Application Facility (OSI SAF). Sea-ice concentration (SIC) is computed from a combination of brightness temperatures from the long-term series of satellite passive microwave instruments SMMR, SSM/I and SSMIS. The product is provided on a 25-km resolution grid but the true spatial resolution is closer to 50 km. The data record contains daily files for the 1979–2015 period, which covers the full-time series of the satellite snow product (section 2.1.1). All daily files and product documentation are available from the OSI SAF web portal (Table 1). More details on the retrieval method and product validation are also found in Lavergne et al. (2019). It must be noted that due to the coarse spatial resolution and potential coastal noise, this product is not meant to monitor the ice cover in the long narrow fjords but mainly represents the conditions in the open adjacent sea.

During winter months, Svalbard is almost encapsulated by sea ice except for the western part with much-reduced sea ice due to the influence of the warm Atlantic water in the West Spitsbergen Current. In the summer months, the ice edge retreats northward and is often completely detached from the coast of Svalbard. Typically, the ice cover is the largest around March, and the sea-ice minimum occurs around September [see Figure 4 (upper two panels)].

In order to investigate how the presence of sea ice might influence the onset and speed of snow melting on land, a time series of daily sea-ice area (SIA) is derived from the SIC data within a region around Svalbard (0–40°E longitude, 72–85°N latitude). SIA is defined as the accumulated area of the ocean surface covered by any amount of ice (with SIC > 0%). Figure 4 (lower left panel) shows the seasonal curves of the Svalbard SIA for 1982–2015 with each year coloured differently. SIA has large seasonal and interannual variabilities; however, an overall trend of decreasing SIA values per decade is visible throughout the year.

Figure 4 (lower right panel) shows the spatial distribution of the concentration trends in June, as computed in each pixel over the 1982–2015 period. June is a typical melting month midway between maximum and minimum ice conditions, and the ice concentrations are seen to be dominated by negative trends (red) in the Svalbard region, especially along the ice edge east of Svalbard into the northern Barents Sea. A dominance of negative trends in the Svalbard region is found for all months in the year with the strongest trends in the mid-winter months of November to February (not shown). The negative trends suggest a more retained ice edge and a less dense ice cover around Svalbard, which, again, may result in more direct interaction between the relatively warm open ocean and the cold winter atmosphere. Section 2.2.3 contains an analysis of the sea ice trends in relation to the trends for the snow cover derived from the satellite dataset.

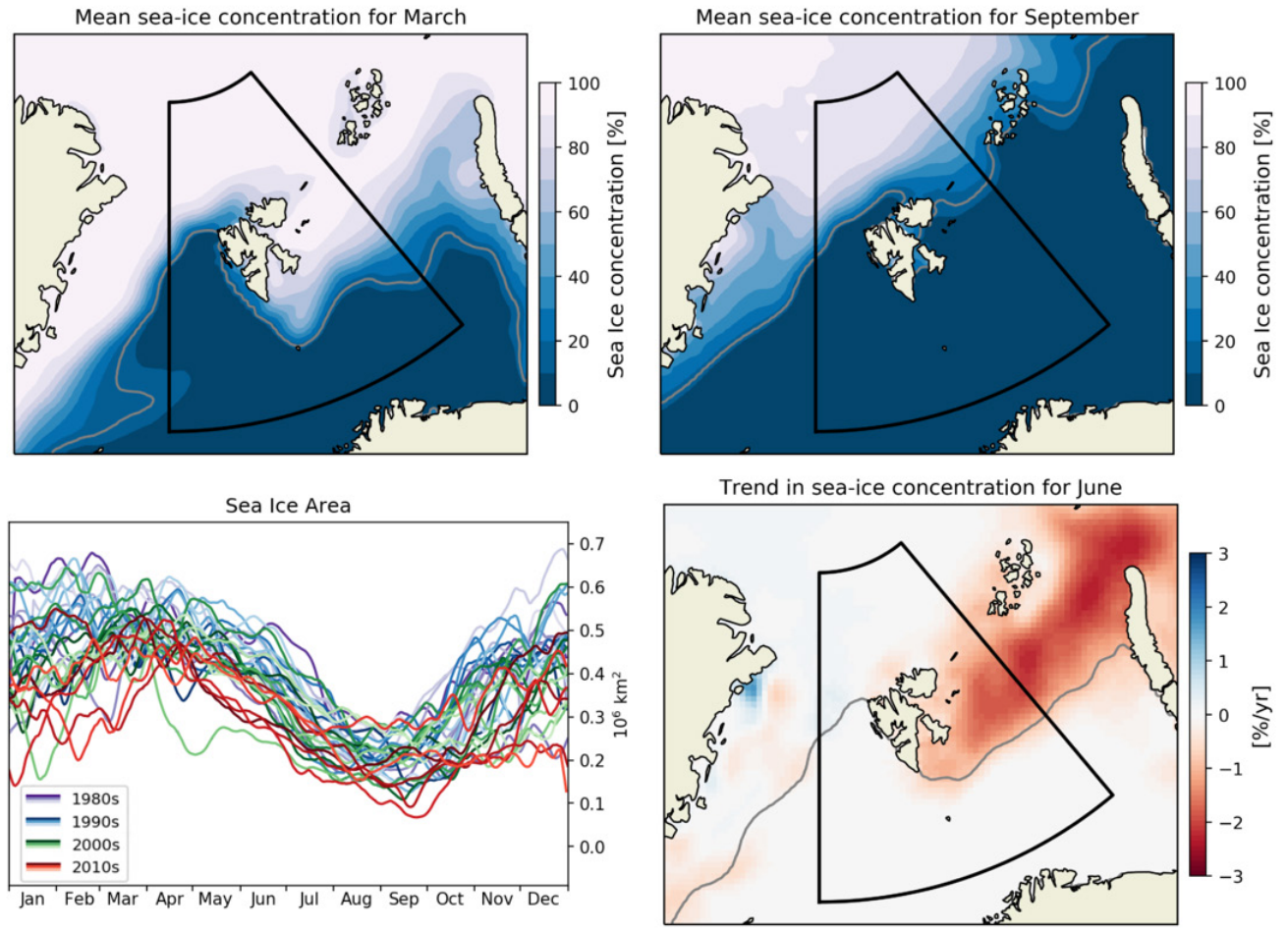

Figure 4: The upper two panels show the mean sea-ice concentration (1982–2015) in March and September, representing the maximum and minimum ice condition around Svalbard. The lower left panel shows the seasonal sea-ice area where each year from 1982 to 2015 is indicated by a separate line. A 9-day moving window average has been applied. The lower right panel shows the trend in the mean sea-ice concentration in June over the 1982–2015 period, with red and blue colours indicating negative and positive trends respectively. For the map plots, the grey contour line along the ice edge represents the 15% line of concentration. The black box on the maps is the Svalbard region over which the sea-ice area is computed. Data source: EUMETSAT OSI SAF global sea-ice concentration climate data record (version 2).

2.2 Data analysis

2.2.1 Comparison of satellite snow with in-situ data

The overlap between the satellite snow cover product (1982–2015) and the in-situ snow-off date data (2010–2015) from COAT is too short for trend analysis, but the comparison and discussion are included here. We focus on three areas on the central Nordenskiöld Land: Gangdalen, Lille Gangdalen and Semmeldalen (see Figure 1). In Figure 5, the upper left panel shows a comparison of the median number of snow-free days from May to July for the in-situ snow-off data for 16 monitoring sites, each within the three areas for each year in 2010–2015 with an average number of SFD from the satellite product collected for a surrounding region (see Figure 1, purple square). Two different elevations are used as maximum, in order to restrict the satellite extract to lower-lying areas. The in-situ monitoring sites are mostly located at or near the base of the valley.

Comparing the ratio of snow-free land according to the satellite product (the LCF) for the same region, as restricted to four different maximum elevations, we find that here the median snow-off date takes place for a low LCF (see Figure 5, upper right panel). The maximum snow-off date corresponds to LCFs in the range of 0.5 to 0.9, depending on the maximum pixel elevation. Considering that the in-situ sites generally represent early snow-off dates, these results are reasonable.

Comparisons are also drawn between the satellite snow product and the in-situ observations of snow cover around Svalbard Airport, as described in section 2.1.3. Satellite data are collected for a region near the weather station (see Figure 1, orange square), and is limited to only contain pixels between sea surface level and up to an elevation of 200 meters. The SCF for this region is shown in Figure 5 (lower left panel) as a function of the day. The median value together with the 10 and 90 percentiles are shown in the same panel (red lines). Blue lines show the median and the 10 and 90 percentiles for the SC code from the in-situ snow data. The lower right panel shows in-situ snow cover data with dashed lines and satellite data with solid lines. Here, the data are gathered in decades, and median values are shown. Both the in-situ snow cover data and the satellite data show a shift towards earlier melting of snow. Svalbard Airport is located at the outermost part of Adventdalen and near the fjord Isfjorden and is exposed to strong winds, which means that it only has a thin snow cover in winter and, like the COAT data, is early snow-free. The observed differences between the satellite product and station data are reasonable.

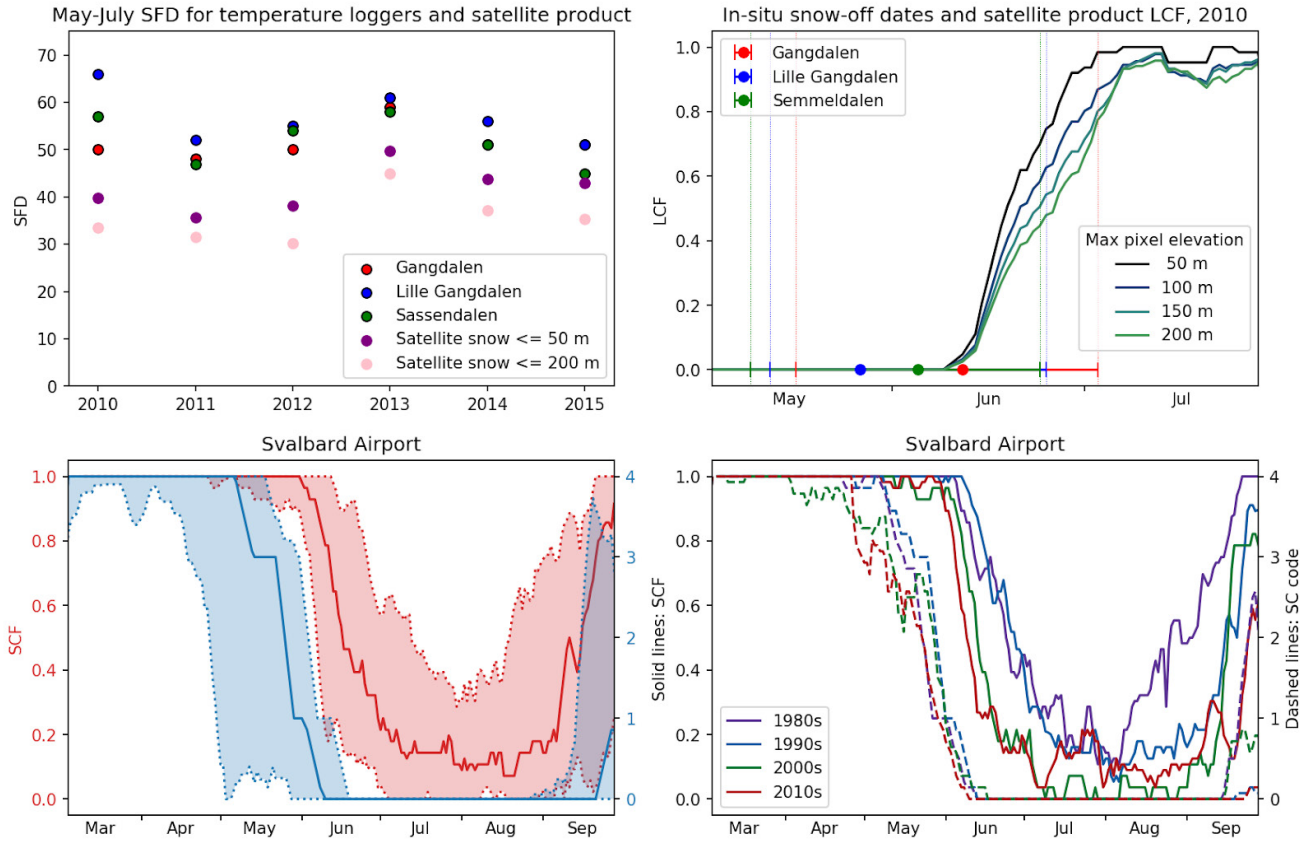

Figure 5: The upper left panel shows the number of SFD during May–July from the in-situ snow-off data from three valleys, using the median values derived from 16 monitoring sites in each of the three valleys. The plot also shows an average number of SFD for the same period from two extracts of the satellite data. One extract (shown in purple) takes unglaciated satellite pixels up to a maximum elevation of 50 meters. The total number of snow-free pixels within the region is summed and divided by the total number of pixels. The process is then repeated with a maximum elevation of 200 meters (shown in pink). The upper right panel shows a comparison of snow-off dates for the iButton loggers with the ratio of snow-free land (the LCF) from the satellite product. The year 2010 is shown here. For the satellite product, 4 maximum elevations are set. The lower panels illustrate comparisons of the satellite snow product with in-situ SC data around Svalbard Airport. The left panel shows the median value for the satellite SCF for the orange square indicated in Figure 1 (averaged over 9 days) together with two percentiles in red, and the median value for the in-situ SC code together with two percentiles in blue. In the lower right panel, the data from the lower left panel are grouped in decades, and median values are shown.

2.2.2 Comparison of snow cover from the satellite with snow model

From the satellite data and the snow model data, the SFD for May–August has been found for each pixel for each year in the 1982–2015 period. Figure 6 compares the averaged total May–August SFD (top) and the trends (bottom). Trends are only shown for the non-glacier domain and for when the trend is significant at a 95% confidence level. Overall, the model and satellite products produce similar spatial patterns of both the average SFD and the associated trends. Both products find the highest SFD (up to 100 days) at low elevations in central Spitsbergen, where the strongest positive trends are also found (up to 2 days per year). The latter high trends, implying a > 60 days increase in snow-free-season length over 1982–2015, can only be explained by the complete melting of multi-year snow patches during the study period. In other parts of Svalbard, trends are mostly non-significant, in part because of high inter-annual variability. A difference between the two products is that, in contrast to the satellite observations, the model SFD trend distribution does not show an alternating pattern of negative and positive trends in central Svalbard, but shows a more homogeneous positive trend.

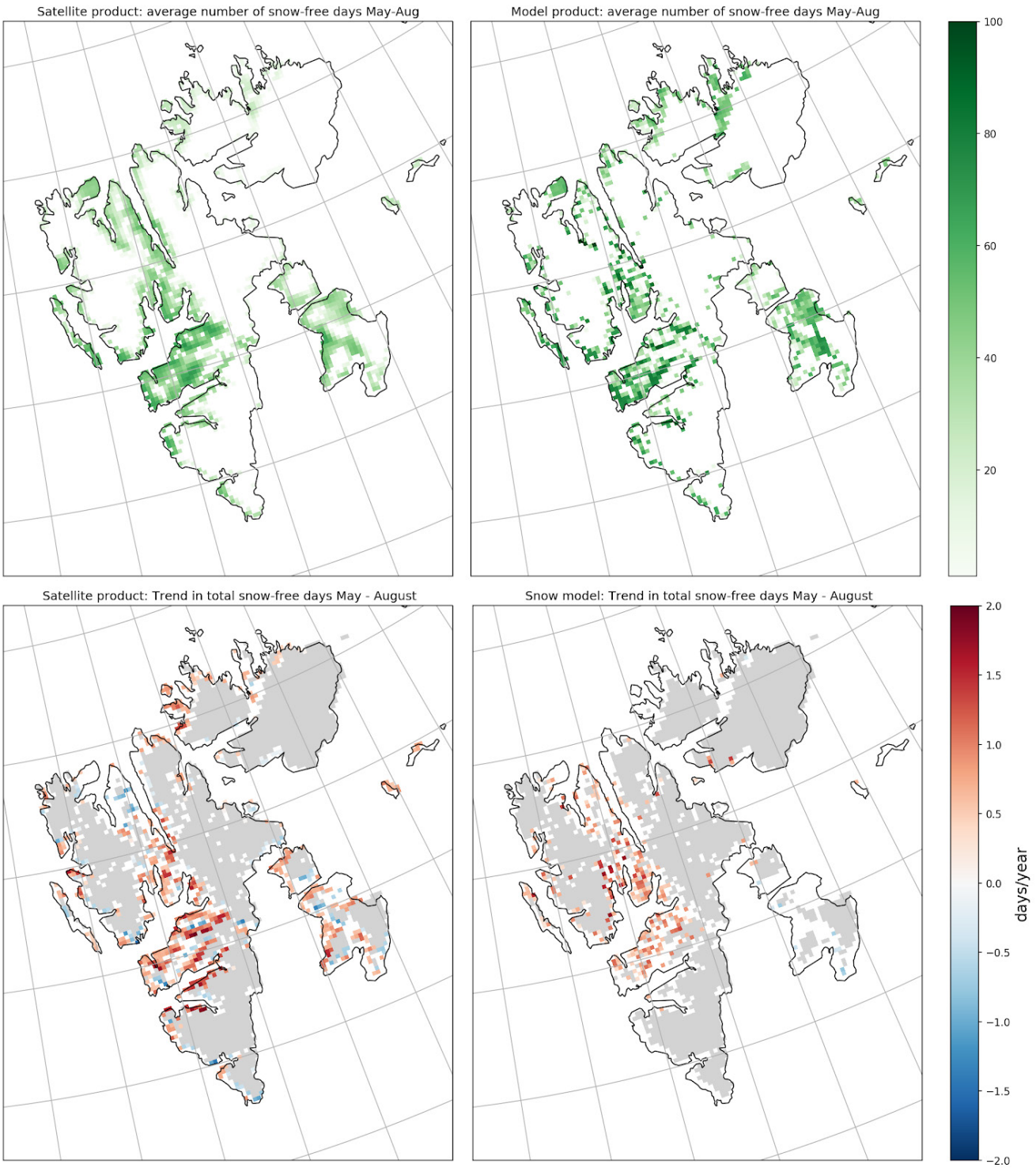

Figure 6: The upper panels show the mean SFD) for May–August over the 1982–2015 period for the satellite product (left) and the snow model interpolated to the satellite grid (right). The lower panels show the trend in total SFD for May–August over the same years, again with the satellite product (left) and snow model (right). Here, glaciated pixels are masked (grey), and only pixels significant to the 5% p-level are coloured.

2.2.3 Correlation between snow on land and sea ice

In the previous sections that presented the long-term satellite datasets of terrestrial snow in Svalbard and sea ice in the adjacent sea, negative trends dominated both datasets over the 34-year period from 1982 to 2015. The onset of snow melting has, on average, advanced more than a week from late June to mid-June, and the sea-ice conditions show dominantly negative trends in the Svalbard region for each month of the year. Despite the long-term negative trends in common, how well does the interannual variability of the snow cover on land and the amount of ice-covered adjacent seas relate to each other? The monthly averaged values of the SIA and SCE are compared with a range of time lag combinations: SCE for May to August against SIA for January to August. Both datasets are linearly detrended in order to avoid high correlation without causation. Instead, we are seeking the correlation of their respective interannual variations.

The first comparison of SIA with SCE, including all land pixels (excluding glaciers), results in positive but non-significant correlations for all time lag combinations. This correlation between sea-ice area and Svalbard total snow cover is also supported by a recent study by Vickers et al. (2020), who compared the Svalbard snow cover based on remote-sensing MODIS data and the regional sea ice in the 2000–2019 period. In the following comparisons, we therefore account for the elevation of the land pixel. The trend in the duration of the snow cover was found to be strongly dependent on the land elevation (Figure 3), and it is thus reasonable to assume that any atmospheric effect from an ice-covered/ice-free ocean will also have a larger influence on the lowlands rather than on the higher mountains where temperatures are colder and often below 0 degrees.

The combinations giving the highest correlations are presented in Figure 7 (left panel) as a function of the selected maximum pixel elevations between 50 m and 250 m a.s.l. Comparison of the SCE for June and SIA for June results in significant positive correlations for all the lowland elevations (green line). A significant positive correlation with a 2-month time lag is also found between SCE (up to 150 m pixel elevation) for June and SIA for April. Beyond that, overall positive correlations are found between SCE for June and SIA for January to March and May, but they may not be significant to a 5% p-level. That the June values of SCE caused the highest correlations against the SIA does not come as a surprise as June represents the time of onset of snow melting, which is again most probably affected by the ocean-air interactions and transport of warmer or colder winds from an open ocean or ice-covered ocean, respectively, over land. The significant linear relationship in June (R=0.45, P=0.009) is shown in the scatter plot in Figure 7 of SIA against SCE for land pixels of maximum 50 m elevation. Both monthly datasets are detrended, and each dot represents a year within the 1982–2015 period, coloured with respect to their decadal affiliation.

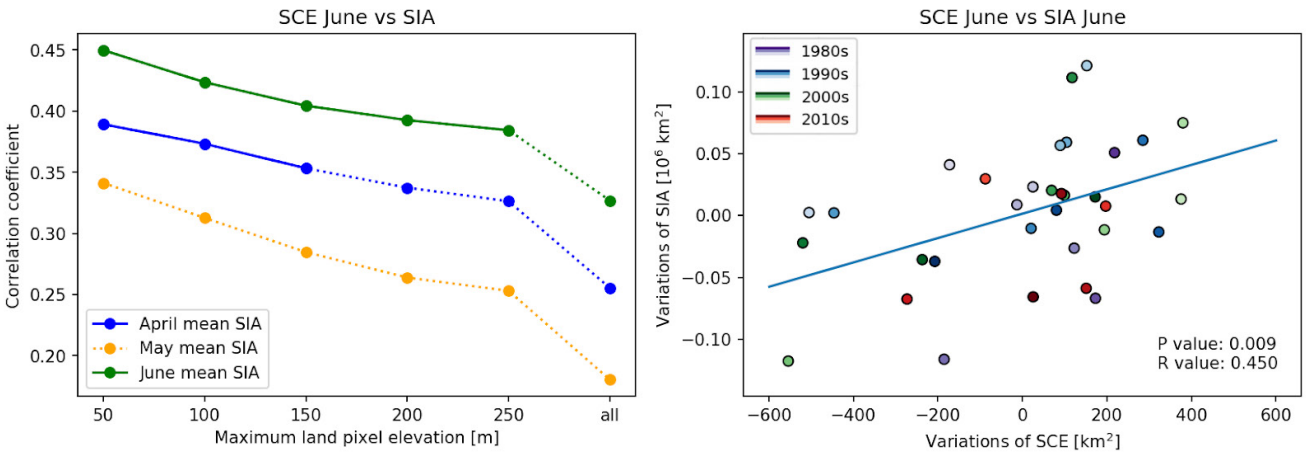

Figure 7: Left panel shows the correlation between the SCE in June and SIA for April, May and June, which gave the highest correlations. Correlations are plotted against the maximum pixel elevation from 50 m to 250 m, and also includes correlation using all land pixels (glacier excluded). The solid line represents when correlation is significant to 5%, whereas the dotted line represents non-significant correlation. Right panel shows the scatterplot of SCE against SIA for June (with no time lag), which had the highest correlation (R=0.45, P=0.009). Each yearly dot is coloured with respect to its decadal affiliation.

3. Connections and synergies with other SESS report chapters

The data and analysis of snow in Svalbard presented in this chapter are related to other chapters in this issue. The chapter "Satellite and modelling–based snow season time series for Svalbard: Inter-comparisons and assessment of accuracy" (Malnes et al. 2021) compares a MODIS-based time series of fractional snow cover (2000–2020) with other satellite-based snow datasets (including the satellite snow time series discussed herein) and with snow models (including the snow model used in this chapter). They focus on differences between the datasets and investigate whether the datasets can build on each other and thereby provide a long-term time series of snow cover data.

The chapter "Terrestrial Photography Applications on Snow Cover in Svalbard (PASSES)" (Salzano et al. 2021) gives an overview of time-lapse camera systems working in Svalbard, with special focus on snow cover applications. The PASSES initiative has managed to identify a large number of image providers, archived imagery and processed datasets dating back to the year 2000. Despite the differences in spatial resolution, the identified time-lapse imagery and fractional snow cover products might be an important source of data for calibration and validation of both snow (Aalstad et al. 2020) and sea ice satellite products.

4. Unanswered questions

Here we list some questions that still remain to be explored to fill the gaps we have identified.

- What are the changes/dynamics in snow cover extent during the polar night period?
- The alternating pattern of negative and positive trends in central Svalbard seen in the satellite product should be investigated. It is not found in the snow model. Is this an artefact, or does it reflect the increase in precipitation seen over Svalbard (cf. Hanssen-Bauer et al. 2019)?
- In the present study, temporal variation in the snow was compared directly with sea-ice area variability. However, how is this relation affected by other geophysical factors such as temperature, wind, and humidity?
- In the analysis of different time-lag combinations between snow and sea ice, a negative correlation was found between late-summer snow and mid-winter sea-ice conditions. This is out of the scope of this chapter, but an unanswered question is whether a reduced sea-ice cover early in the year might affect a long-lasting snow cover in Svalbard. Could it be a chain reaction where less ice causes more ocean–air interaction, thereby causing more humidity over land, which again results in more snow precipitation?

5. Recommendations for the future

Focus on snowpack properties: The ecosystem impact of changing snowpack properties, snow cover extent and duration in a warming climate is a particularly central theme in COAT and a generally important arena for interdisciplinary research between ecology and geophysics. Besides the need for co-location of research infrastructure, there is a need to develop a data-model fusion system that merges available observational datasets on snow properties with state-of-the-science, high-resolution (1- to 500-meter scale), physically based snow models. The goal of this data-enhancement system is to create accurate, spatially distributed and time evolving datasets that can be used to better understand relationships between drivers (predictors) and biotic responses and ecosystem processes. Several climate impact pathways formalized by COAT conceptual models are driven by changes in snowpack properties, snow cover extent and duration. State-of-the-art monitoring of such pathways is dependent on snow modelling products, and joint efforts will contribute to this. See further details in Pedersen et al. (2020).

Focus on spatially and temporally explicit sea-ice maps: Wildlife use sea ice as hunting and migration corridors, and the lack of high-quality maps at the relevant spatial and temporal scales relevant to wildlife is hampering the possibility of analysing data at ecologically relevant scales to the long-term monitoring of climate change effects of the COAT program. Such products may also be essential in the continuation of understanding the linkages between sea ice and terrestrial primary productivity (Macias-Fauria et al. 2017).

Strengthen the collaboration: The scientific community will benefit from a more coordinated cooperation between snow research groups operating in and outside the SIOS infrastructures and the wider snow remote sensing community. Remote sensing products need high-quality calibration and validation data series. Discovery and assimilation of archival and on-going snow depth, snow water equivalent and snow cover extent datasets (especially archival, dating back to the 80's) would be extremely helpful in calibration and validation of long-term satellite products and models.

6. Data availability

Table 1 contains a list of the datasets used, including the data owner and how to access the data.

Table 1: A list of the datasets used in this study

Dataset	Parameters	Period	Location	Metadata/Data Access	Data provider, reference
1982–2015 daily, binary snow cover maps for Svalbard	Snow cover	1982–2015	Svalbard archipelago	Available in the SIOS data access portal in Q1 2021	MET Norway
COAT data	Snow-off dates derived from temperature loggers (iButton)	2010–2015	Nordenskiöld Land	COAT database (not published yet)[1] Research/Data/ COAT-Data-Portal	NMBU (Leif Egil Loe)
Snow cover data from the Svalbard Airport	Manually observed in-situ data -	1982–2015	The manned station at Svalbard Airport	frost.met.no	MET Norway
A long-term model dataset of climatic mass balance, snow conditions and runoff in Svalbard (1957–2018)	SFD extracted from modelled SWE data	1982–2015	Svalbard archipelago	SIOS data access portal: https://bit.ly/3fG7pAZ	Uppsala University https://doi.org/10.5194/tc-13-2259-2019, https://doi.org/10.6084/m9.
Global sea-ice concentration climate data record 1979–2015 (v2.0, 2017), OSI-450	Sea-ice concentration from passive microwave data (SMMR/ SSMI/SSMIS). Grid resolution of 25 km.	1982–2015	Northern Hemisphere	EUMETSAT OSI SAFdoi: 10.15770/ EUM_SAF_ OSI_0008, Data extracted: 1982-2015, 72-85N 0-40E, accessed Sep 2020.	http://osi-saf.eumetsat.int

Acknowledgements

This work was supported by the Research Council of Norway, project number 291644, Svalbard Integrated Arctic Earth Observing System – Knowledge Centre, operational phase. We thank Leif Egil Loe, NMBU, for use of the temperature logger data for this purpose.

1 https://www.coat.no/en/

References

Aalstad K, Westermann S, Bertino L (2020) Evaluating satellite retrieved fractional snow-covered area at a High Arctic site using terrestrial photography. Remote Sens Environ 239:111618. https://doi.org/10.1016/j.rse.2019.111618

EUMETSAT Ocean and Sea Ice Satellite Application Facility, Global sea ice concentration climate data record 1979-2015 (v2.0, 2017), OSI-450. doi: 10.15770/EUM_SAF_OSI_0008, Data extracted: 1982-2015, 72-85N 0-40E. Accessed 8 September 2020.Hansen BB, Isaksen K, Benestad RE, Kohler J, Pedersen ÅØ, Loe LE, Coulson SJ, Larsen JO, Varpe Ø (2014) Warmer and wetter winters: characteristics and implications of an extreme weather event in the High Arctic. Environ Res Lett 9:114021. https://doi.org/10.1088/1748-9326/9/11/114021

Hanssen-Bauer I, Førland EJ, Hisdal H, Mayer S, Sandø AB, Sorteberg A (eds.) (2019) Climate in Svalbard 2100 – a knowledge base for climate adaptation, NCCS Report No. 1/2019. https://www.miljodirektoratet.no/globalassets/publikasjoner/M1242/M1242.pdf

Ims RA, Jepsen JU, Stien A, Yoccoz NG (2013) Science plan for COAT: Climate-ecological Observatory for Arctic Tundra. Fram Centre, Tromsø. https://www.coat.no/en/Publications/COAT-science-plan

Killie MA (2019) Validation of a Satellite based snow cover index for Svalbard. Project report for SIOS ACCESS project 2018_0007. https://sios-svalbard.org/sites/sios-svalbard.org/files/common/SvalSCE_2018_0007_correctedfigure.pdf

Killie MA, Godøy Ø, Eastwood S, Lavergne T (2011) Algorithm theoretical basis document for the EUMETSAT ocean & sea ice satellite application facility regional ice edge product. Ocean & Sea Ice SAF project report no. OSI-146, Version 1.2.

Lavergne T, Sørensen AM, Kern S, Tonboe R, Notz D, Aaboe S, Bell L, Dybkjær G, Eastwood S, Gabarro C, Heygster G, Killie MA, Kreiner MB, Lavelle J, Saldo R, Sandven S, Pedersen LT (2019) Version 2 of the EUMETSAT OSI SAF and ESA CCI sea-ice concentration climate data records. The Cryosphere 13:49–78. https://doi.org/10.5194/tc-13-49-2019

Loe LE, Hansen BB, Stien A, Albon SD, Bischof R, Carlsson A, Irvine RJ, Meland M, Rivrud IM, Ropstad E, Veiberg V, Mysterud A (2016) Behavioral buffering of extreme weather events in a high-Arctic herbivore. Ecosphere 7:1. https://doi.org/10.1002/ecs2.1374

Luce CH, Tarboton DG, Cooley KR (1998) The influence of the spatial distribution of snow on basin-averaged snowmelt. Hydrol Process 12:1671–1683. https://doi.org/10.1002/(SICI)1099-1085(199808/09)12:10/11<1671::AID-HYP688>3.0.CO;2-N

Macias-Fauria M, Karlsen SR, Forbes BC (2017) Disentangling the coupling between sea ice and tundra productivity in Svalbard. Sci Rep. 7 8586 *https://doi.org/10.1038/s41598-017-06218-8*

Malnes E, Vickers H, Karlsen SR, Saloranta T, Killie MA, Van Pelt W, Pohjola V, Zhang J, Stendardi L, Notarnicola C (2021) Satellite and modelling based snow season time series for Svalbard: Inter-comparisons and assessment of accuracy. In: Moreno-Ibáñez et al (eds) SESS report 2020, Svalbard Integrated Arctic Earth Observing System, Longyearbyen, pp. 202 – 219. https://sios-svalbard.org/SESS_Issue3

Mott R, Gromke C, Grünewald T, Lehning M (2012) Relative importance of advective heat transport and boundary layer decoupling in the melt dynamics of a patchy snow cover. Adv Water Resour 55:88–97. https://doi.org/10.1016/j.advwatres.2012.03.001

Pedersen ÅØ, Stien J, Albin S, Fuglei E, Isaksen K, Liston G, Jepsen JU, Madsen J, Ravolainen VT, Reinking AK, Soininen EM, Stien A, van der Wal R, Yoccoz NG, Ims RA (2020) COAT – Climate-ecological Observatory for Arctic tundra. In: Van den Heuvel et al. (eds): SESS report 2019, Svalbard Integrated Arctic Earth Observing System, Longyearbyen, pp. 58–83 . https://sios-svalbard.org/SESS_Issue2

Salzano R, Aalstad K, Boldrini E, Gallet JC, Kępski D, Luks B, Nilsen L, Salvatori R, Westermann S (2021) Terrestrial photography applications on snow cover in Svalbard. In: Moreno-Ibáñez et al (eds) SESS report 2020, Svalbard Integrated Arctic Earth Observing System, Longyearbyen, pp. 236 – 251. https://sios-svalbard.org/SESS_Issue3

Staub B, Delaloye R (2017) Using near-surface ground temperature data to derive snow insulation and melt indices for mountain permafrost applications. Permafr. Periglac. Process 28:237–248. https://doi.org/10.1002/ppp.1890

Van Pelt WJJ, Oerlemans J, Reijmer CH, Pohjola VA, Pettersson R, Van Angelen JH (2012) Simulating melt, runoff and refreezing on Nordenskiöldbreen, Svalbard, using a coupled snow and energy balance model. The Cryosphere 6:641–659. https://doi.org/10.5194/tc-6-641-2012

Van Pelt W, Kohler J (2015) Modelling the long-term mass balance and firn evolution of glaciers around Kongsfjorden, Svalbard. J Glaciol 61:731–744. https://doi.org/10.3189/2015JoG14J223

Van Pelt W, Pohjola V, Pettersson R, Marchenko SA, Kohler J, Luks B, Hagen JOM, Schuler T, Dunse T, Noel B, Reijmer C (2019) A long-term dataset of climatic mass balance, snow conditions, and runoff in Svalbard (1957–2018). The Cryosphere 13:2259–2280. https://doi.org/10.5194/tc-13-2259-2019

Vickers H, Karlsen SR, Malnes E (2020) A 20-year MODIS-based snow cover dataset for Svalbard and its link to phenological timing and sea ice variability. Remote Sens. 12:1123. https://doi.org/10.3390/rs12071123